Published in final edited form as:
Dalton Trans. 2016 August 02; 45(31): 12539–12547. doi:10.1039/c6dt02177h.

Design and synthesis of novel organometallic dyes for NiO sensitization and photo-electrochemical applications

Julien Massin[a], **Siliu Lyu**[b], **Michele Pavone**[c], **Ana B. Muñoz-García**[c], **Brice Kauffmann**[d], **Thierry Toupance**[b], **Murielle Chavarot-Kerlidou**[a], **Vincent Artero**[*,a], and **Céline Olivier**[*,b]

[a]Laboratoire de Chimie Biologie des Métaux, Université Grenoble Alpes, CNRS UMR 5249, CEA Fundamental Research Division, Grenoble, France

[b]Institut des Sciences Moléculaires, Université de Bordeaux, CNRS UMR 5255, Talence, France

[c]Department of Chemical Sciences, University of Naples Federico II, Napoli, Campania, Italy

[d]Institut Européen de Chimie et Biologie, Université de Bordeaux, UMS CNRS-INSERM 3033, Pessac, France

Abstract

Two metallo-organic dyes were synthesized and used for NiO sensitization in view of photoelectrochemical applications. The new dyes present an original **π**-conjugated structure including the [Ru(dppe)$_2$] metal fragment with a highly delocalized allenylidene ligand on one side and a **σ**-alkynyl ligand bearing an electron-rich group, i. e. thiophene or triphenylamine unit, and one or two anchoring functions, on the other side. The optoelectronic, electrochemical and photoelectrochemical properties of the dyes were systematically investigated. A broad photoresponse was observed with absorption maximum at 600 nm. The X-ray crystal structure of one precursor was obtained to elucidate the structural conformation of the organometallic complexes and theoretical calculations were performed in order to address the photophysical properties of the new dyes. These photosensitizers were further implemented into NiO-based photocathodes and tested as photocurrent generators under pertinent aqueous conditions in association with [Co(NH$_3$)$_5$Cl]Cl$_2$ as an irreversible electron acceptor. The dye-sensitized photocathodes provided good photocurrent densities (40 to 60 μA cm^{-2}) at neutral pH in phosphate buffer and a high stability was observed for the two dyes.

Introduction

Sunlight is by far the most abundant renewable energy source. Its storage, however, remains a grand challenge which would allow a secure energy scenario for our society.[1–3] The production of fuels from solar energy and other renewable raw materials is probably the most promising solution in that prospect. As a first target, molecular hydrogen can be produced from water splitting, producing O_2 as a side product. The light-driven reduction of CO_2 can also produce carbon-based fuels, with a net zero-carbon footprint. Technologically, these processes can be implemented in photoelectrochemical cells (PEC).[4,5] Various

* vincent.artero@cea.fr, celine.olivier@u-bordeaux.fr.

Europe PMC Funders Author Manuscripts

architectures have been designed for such devices, all containing photoelectrodes.[6] In this context, visible-light driven hydrogen production from photoactive cathodes based on molecular catalysts and dye-sensitized metal oxide semiconductor is of great interest.[6,7] By analogy with *p*-type dye-sensitized solar cells (p-DSSCs),[8,9] NiO-based photocathodes were obtained by sensitization of nanostructured thin films with organic or metallo-organic dyes and displayed photoelectrochemical activity in aqueous media.[10–16]

In such photocathodes the dye plays a crucial role for the collection of sunlight and the inception of electron-transfer processes. In the present study, we focused on the design and preparation of innovative dye structures with suitable redox properties. The dyes were further implemented into NiO-based photocathodes and tested as photocurrent generators under pertinent aqueous conditions in association with an irreversible electron acceptor (IEA).

Some of us recently reported the preparation and study of asymmetric ruthenium-diacetylide organometallic complexes as efficient photosensitizers for TiO_2 in *n*-type DSSCs[17,18] and for NiO in p-type DSSCs.[19] Besides, another type of organometallic complexes including the [Ru(dppe)$_2$] core has been previously reported, namely mixed alkynyl-allenylidene complexes.[20,21] Such highly conjugated architectures intrinsically present excellent visible-light absorption properties over a broad wavelength range and low bandgap energy. Accordingly, the dyes targeted in this study present a mixed alkynyl-allenylidene structure as represented in Chart 1. In addition to the electron-rich [Ru(dppe)$_2$] metal centre, the photosensitizer **[Ru]1** presents an electron-donating thiophene ring equipped with one carboxylic acid anchoring function while the dye **[Ru]2** presents two carboxylic acid functions on a triphenylamine motif. The optical and electronic properties of the new dyes were thoroughly characterized showing that mixed alkynyl-allenylidene ruthenium complexes are promising sensitizers for NiO with the aim of producing stable photoelectrochemical systems.

Results and discussion

Synthesis and characterization

The synthetic route to the new dyes **[Ru]1** and **[Ru]2** is depicted in Scheme 1. Synthesis of the alkynyl ligands bearing the anchoring groups involved Sonogashira coupling reaction of appropriate halogenated precursors with trimethylsilylacetylene and subsequent deprotection of the terminal alkyne. The carboxylic acid anchoring functions were endowed with a silyl-ester protecting group, i. e. 2-(trimethylsilyl)ethyl (TMSE), in order to avoid side reactions with the metal centre during the following reactions steps towards organometallic complexes. Thus, according to the general procedure previously described for the synthesis of [Ru(dppe)$_2$] metal complexes,[21] activation of the terminal alkynes **2** or **5** by the 16-electron species [RuCl(dppe)$_2$][TfO] led to the corresponding stable ruthenium-vinylidene moieties **3** and **6**. Subsequent reaction of the latter with a slight excess of propargyl-alcohol HC≡C–CPh$_2$OH, in the presence of a non-coordinating salt ($NaPF_6$) and a base (Et_3N), allowed substitution of the chlorine atom on the [Ru(dppe)$_2$] core and introduction of the second carbon-rich chain. Spontaneous dehydration of the alkynol ligand under those reaction conditions led to the cumulenic chain =C=C=CPh$_2$, thus affording the dye

precursors **4** and **7**. Final deprotection of the silyl-ester group(s) under mild conditions, using tetrabutyl ammonium fluoride in THF and at room temperature, afforded the target dyes **[Ru]1** and **[Ru]2** in good yields. All the organometallic complexes were characterized by means of ^{31}P, ^{1}H and ^{13}C NMR, HR-MS and FTIR. The *trans*-ditopic structure of the ruthenium center in **[Ru]1** and **[Ru]2** was first confirmed by the ^{31}P NMR spectra which show a singlet for the four equivalent phosphorus atoms, with $\delta \approx 43$ ppm characteristic of the mixed Ru-alkynyl-allenylidene structure.[20,21] The presence of an allenylidene carbon-rich chain was also evidenced by characteristic ^{13}C NMR signals at $\delta \approx 316$ (C_α), 212 (C_β) and 162 (C_γ) ppm and by a typical intense vibration stretch ($\nu_{C=C=C}$) on the IR spectra at ˜ 1917 cm^{-1}. A less intense vibration stretch, characteristic of the alkynyl ligand ($\nu_{C\equiv C}$), was also observed on the IR spectra at ˜ 2063 cm^{-1}.

Crystallographic study

Good quality crystals were obtained by slow diffusion of pentane into a concentrated solution of the complex **4** in CH_2Cl_2 solution. The crystal structure of **4** was thus resolved by X-ray diffraction analyses. Fig. 1 represents the cationic organometallic unit from different views along with appending triflate anion. The crystallographic data are detailed in the supporting information. The crystal structure of **4** confirms the *trans* position of the two carbon-rich ligands with regard to the metal centre, providing a linear arrangement of the carbon chains with an angle C_α–Ru–$C_\alpha{}'$ = 179.1(7)°. The linearity of the chains extends well beyond, over 9.27 Å from the C_γ to the $C_{\gamma'}$, with an angle C_γ–Ru–$C_{\gamma'}$ = 178.7(2)°. The different bond lengths are consistent with the presence of a cumulenic chain on one side and an alkynyl chain on the other side.[20] The corresponding distances are 1.933, 1.261 and 1.364 for the Ru–C_α, C_α–C_β and C_β–C_γ of the allenylidene ligand, and 2.081, 1.197 and 1.436 for the Ru–$C_\alpha{}'$, $C_\alpha{}'$–$C_\beta{}'$ and $C_\beta{}'$–$C_\gamma{}'$ of the acetylide ligand. Note that the Ru-C_α distance is longer in the alkynyl chain than in the cumulenic one, and conversely the C_α–C_β is much shorter in the alkynyl ligand, thus presenting a strong C≡C character. The crystal structure also shows how the metal atom and linked carbon chains are surrounded by the diphosphine ligands which shelter the central π-conjugated system and, through their bulkiness, create a de-aggregating effect.

Optical and electrochemical properties

UV-visible electronic absorption spectra of the dyes, recorded in dichloromethane solution, are presented in Fig. 2 and the corresponding data are gathered in Table 1. On these spectra, intense absorption bands are observed in the UV region, below 300 nm, corresponding to n → π* and π → π* transitions characteristic of the dppe ligands.[22] The spectra also show intense absorption bands at intermediate energy with maximum wavelength centred at 340-350 nm. These bands are tentatively attributed to transitions involving the electron-rich alkynyl ligand. The polyaromatic triphenylamine motif provides a twice more intense band (ε = 41 000 M^{-1} cm^{-1}) than the thiophene ring (ε = 20 100 M^{-1} cm^{-1}). More interestingly, the spectrum of both dyes shows a very broad absorption band in the visible region with maximum wavelength located at $\lambda_{max} \approx 600$ nm and $\varepsilon \approx 12\,000$ M^{-1} cm^{-1}. In mono-allenylidene metal complexes the transition in the visible region possesses a metal-ligand charge transfer (MLCT) character of the type Ru^{II}(dπ) → π*(allenylidene).[23] Similarly, the broad absorption observed for **[Ru]1** and **[Ru]2** in the visible is expected to arise from

the allowed transition from one of the metal-based orbitals (HOMO) to the allenylidene-ligand-based LUMO.

Cyclic voltammetry analyses of the organometallic complexes were performed in dichloromethane solution, the corresponding data are reported in Table 1. The cationic allenylidene-acetylide complexes show a well-defined reversible mono-electronic wave located at – 0.99 V and – 0.89 V *vs.* Fc^+/Fc for **[Ru]1** and **[Ru]2**, respectively. This electronic process is ascribed to the reduction of the cumulenic ligand.[21] Assuming that these potentials are not significantly affected when shifting from dichloromethane to acetonitrile[24] and considering $E^0_{(Fc+/Fc)}$ = + 0.53 *vs.* NHE in CH_3CN,[15,25] we could estimate the LUMO energy level of the dyes to – 4.11 eV and – 4.21 eV for **[Ru]1** and **[Ru]2**, respectively.

The HOMO energy level was calculated accordingly by subtracting the optical bandgap energy to the LUMO energy, $E_{HOMO} = E_{LUMO} - E_{0\text{-}0}$. The HOMO energy was therefore estimated at *ca.* – 5.7 eV for **[Ru]1** and **[Ru]2**. As a consequence, the HOMO energy level of the dyes is lower than the edge of the valence band of NiO ($E_{VB\ (NiO)}$ = – 5.0 eV)[27–29] indicating that sufficient driving force exists for hole injection from the photoexcited dyes to the semiconducting metal-oxide. On the other hand, the electron promoted to the LUMO upon photoexcitation is at sufficiently high energy to be transferred to an irreversible electron acceptor (IEA) such as $[Co(NH_3)_5Cl]Cl_2$($E^0_{Co(III)/Co(II)}$ = – 4.5 eV).[30] In that configuration, photoinduced electron transfers from NiO to the IEA, mediated by the mixed allenylidene-acetylide ruthenium complexes **[Ru]1** and **[Ru]2**, should be highly favourable.

Theoretical calculations

Quantum chemical calculations were performed in order to get deeper insight into the molecular orbital distribution and the electronic transitions occurring upon photoexcitation of the dyes **[Ru]1** and **[Ru]2**. Spatial representation of the frontier molecular orbitals HOMO and LUMO calculated at the PBE0 level of theory is shown in Fig. 3 (see Experimental Part for details).

The calculations show that the HOMO (Highest Occupied Molecular Orbital) of the dyes is delocalized over the acetylide ligand bearing the thiophene (**[Ru]1**) or triphenylamine unit (**[Ru]2**) and on the anchoring group(s), which should greatly favour hole injection into the valence band of NiO.[31] The HOMO also displays a strong contribution from the metal centre, and in the case of **[Ru]1** a substantial extension onto the cumulenic carbon chain. On the other hand the LUMO (Lowest Unoccupied Molecular Orbital) of such mixed allenylidene-acetylide metal complexes is mainly localized on the allenylidene ligand thus involving the external phenyl rings, the cumulenic chain and also some contribution from the metal fragment. As a consequence the HOMO and LUMO of the dyes are well positioned on the metal complexes for hole injection into NiO on one side and electron donation to the cobalt-based electron acceptor on the other side.

DFT and TD-DFT calculation parameters relative to the main photoinduced transitions are summarized in Table 2. In accordance with the experiment, two main transitions are predicted for **[Ru]1** and **[Ru]2** in the 300–800 nm region. The maximum wavelengths and

oscillator factors calculated for the two main transitions are consistent with the experimental spectra, the expected small deviation between calculated and experimental data is attributable to the large size of such organometallic complexes and to the well-known limits of TD-DFT for charge-transfer excitations.[32] The maximum wavelength calculated for lowest energy transition is of 676 nm and 687 nm for **[Ru]1** and **[Ru]2**, respectively corresponding to pure charge transfer. We have also analysed the electronic-density rearrangement upon excitation (Fig. S1) and the computed average charge-transfer distance (D_{CT}) is similar for both dyes, with a slightly longer extent for **[Ru]2** than **[Ru]1**. Furthermore the calculated energy of the HOMO is consistent with the one obtained experimentally, i. e. $E_{HOMO\ calc.} = -5.6$ eV *vs.* $E_{HOMO\ exp.} = -5.7$ eV for **[Ru]1** and $E_{HOMO\ calc.} = -5.4$ eV *vs.* $E_{HOMO\ exp.} = -5.7$ eV.

Transition assignment reveals that this low-energy transition owns a major HOMO → LUMO character whereas the transition at higher energy owns a HOMO–1 → LUMO character. These transitions therefore present a net MLCT (Metal-to-Ligand Charge Transfer) character since both the HOMO and HOMO–1 strongly involve the central ruthenium-based fragment. This is further confirmed by the calculated quantity of transferred charge (q_{CT}) which is very close to 1,.

Electrode preparation and characterization

The NiO substrates were purchased from Dyenamo[16] and sensitized by soaking into a 0.5 mM CH_3CN solution of **[Ru]1** or **[Ru]2** for 24 hours. The samples were rinsed with CH_3CN and dried in the air before characterization. Fig. 4a displays typical absorbance spectra of a dye-sensitized electrode, showing new features as compared with the spectrum of the blank NiO substrate (measured on the same sample before sensitization) that correspond to the absorbance of **[Ru]1** or **[Ru]2** dyes grafted onto the NiO surface (Fig. 4b and 4c). For both dyes, a blue-shift (33 nm for **[Ru]1** and 53 nm for **[Ru]2**) of the absorbance band is observed, in agreement with previous reports.[26,28] These modifications result either from small structural rearrangements of the dye molecules upon grafting on the NiO substrate or from intermolecular interactions between adjacent grafted dyes.

First-principles calculations of Coumarin-based dyes (C343) adsorbed on the p-NiO(100) surface have shown that there is no charge-transfer between dye and electrode upon formation of the C343-NiO bonds.[33] In other words, the dye retained its electronic structure features upon adsorption on p-NiO. Since **[Ru]1** and **[Ru]2** dyes are anchored to the NiO surface with carboxylic acid groups as the C343 dye, we assume that the dye-NiO interactions do not significantly modify the molar absorbance coefficient ε_{max} of the dyes. Thus, we estimated the surface concentration of **[Ru]1** and **[Ru]2** using the following equation:

$$surf.conc.(mol.cm^{-2}) = \frac{Abs_{\max}}{1000 x \varepsilon_{\max}(M^{-1}cm^{-1})}$$

This methodology afforded surface concentration estimations of 21.5 ± 0.8 and 28.7 ± 0.8 $nmol.cm^{-2}$ for **[Ru]1** and **[Ru]2** respectively, as average values determined for 3 samples

minimum. Variation in the grafting density between the two dyes likely reflects the fact that **[Ru]2** possesses two carboxylate anchoring groups whereas **[Ru]1** has only one.

Photoelectrochemical properties of dye-sensitized NiO films

The photoelectrochemical properties of the dye-sensitized NiO films were subsequently investigated in the presence of $[Co(NH_3)_5Cl]Cl_2$ (20 mM) acting as an irreversible electron acceptor (IEA) in solution.[15,34] The substrates were used as working electrode in a three-electrode configuration (see the experimental section). Potassium phosphate buffer (KPi, pH 7; 0.1 M) was used as electrolyte and linear sweep voltammograms (LSV) were recorded under chopped-irradiation conditions (400 – 800 nm filtered Xe Lamp light; 100 mW cm^{-2}) corresponding to the visible fraction of 1.5 sun (Fig. 5a). A photocurrent is established with onset at + 0.78 V *vs.* NHE. Such a behaviour is directly related to the presence of **[Ru]1** or **[Ru]2** at the surface of the films since non-sensitized NiO films show very little photocurrent under the same conditions. It is attributed to the establishment of photoinduced electron transfers from NiO to IEA, mediated by the excited dyes. Maximum photocurrent densities (~40 μA cm^{-2} for **[Ru]1** and ~60 μA cm^{-2} for **[Ru]2**) are obtained from + 0.20 V *vs.* NHE (0 V *vs.* Ag/AgCl).[35]

We therefore applied this potential for the whole series of experiments described below. Under such conditions, NiO electrodes sensitized with **[Ru]2** display significantly higher photocurrent density (58 μA cm^{-2}) than the same electrode sensitized with **[Ru]1** (43 μA cm^{-2}) (Fig. 5b). This difference is directly related to the observed difference in surface concentration. Indeed, if the macroscopic photocurrent (μA cm^{-2}) is divided by the Faraday constant and by the surface concentration (nmol cm^{-2}), similar photoinduced molecular electron transfer frequencies of 0.020 and 0.021 s^{-1} are calculated for **[Ru]1** and **[Ru]2**, respectively, suggesting that the two dyes have the same intrinsic efficiency for light-driven charge transfer. In the course of long-term illumination experiments, both electrodes display quite stable photocurrent values for the first 20-30 min. (Fig 5c). After this time, photocurrent values begin to decrease (30 % after one hour for the NiO electrode sensitized by **[Ru]2** and >50% in the case of **[Ru]1** that only contains one anchoring carboxylate group). This behaviour could be ascribed both to the leaching of the dye and to the deposition of an insoluble product at the surface of the electrode, clogging the electrode pores and limiting performances. We note that this deposit likely originates from the decomposition products of the IEA. Such an issue should not take place if a catalyst is used instead of an IEA. These observations contrast with measurements made with an analogous organic push-pull dye containing a triarylamine donor similarly anchored onto NiO through carboxylate groups.[15] Photocurrent values were found very unstable in phosphate buffer, which was ascribed to the leaching of the dye. The good stability of photocurrent at pH 7 for **[Ru]2**-sensitized NiO electrodes therefore holds promises for the development of photoelectrodes for H_2 evolution since most molecular catalysts work under such conditions.[13,14]

Conclusions

Dye-sensitized photocathodes displaying stable photoelectrochemical properties at neutral pH are targeted for the development of H_2-evolving photoelectrocatalytic cells. Tandem cells combining two dye-sensitized photoelectrodes were indeed recently shown capable to split water in absence of any external bias.[13,14] Optimization of the cell performances is now required and includes the design of novel dyes. We show here the relevance of push-pull organometallic dyes for the construction of photocathodes operating in water. The high stability displayed by these new dye-sensitized photocathodes in pH 7 phosphate buffer represents an important improvement compared to the previous photoelectrodes reported in our group[15] and holds promises for the construction of H_2-evolving photoelectrodes through catalysts integration.

Experimental Section

Materials and methods

The reactions were carried out under inert atmosphere using the Schlenk techniques. Solvents were dried from appropriate drying agents (sodium for pentane, diethyl ether and THF; calcium hydride for dichloromethane, chloroform and methanol) and freshly distilled under nitrogen before use. All reagents were obtained from commercially available sources and used without further purification. [RuCl(dppe)$_2$][[TfO] (**1**)[36] and **5** [19] were synthesized according to reported procedures.

^{1}H NMR, ^{13}C NMR and ^{31}P NMR analyses were performed on Bruker Avance I 300 MHz, Avance II 400 MHz and Avance III 600 MHz spectrometers. Chemical shift values are given in ppm with reference to solvent residual signals. HR-MS analyses were performed by the CESAMO (Bordeaux, France). Field desorption (FD) measurements were carried out on a TOF mass spectrometer AccuTOF GCv using an FD emitter with an emitter voltage of 10 kV. One to two microliters solution of the compound were deposited on a 13μm emitter wire. FT-IR spectra were recorded on a Perkin Elmer Spectrum 100 spectrometer using KBr pellets. UV-visible absorption and emission fluorescence spectra were recorded on a UV-1650PC SHIMADZU spectrophotometer and on a FluoroMax-4 HORIBA spectrofluorometer, respectively. Cyclic voltammetry analyses were performed using a potentiostat/galvanostat Autolab PGSTAT100 and a three-electrode system (working electrode: Pt disc; reference electrode: Ag/AgCl, calibrated with decamethylferrocene as internal reference; counter electrode: Pt) with 0.1M Bu_4NPF_6 as salt support at a scan rate of 100 mV.s^{-1}.

Synthesis of 3—In a Schlenk tube under inert atmosphere, [RuCl(dppe)$_2$][TfO] (**1**) (865 mg, 0.8 mmol, 1 equiv.) and **2** (300 mg, 1.2 mmol, 1.5 equiv.) were dissolved in dry CH_2Cl_2 (50 mL). The mixture was stirred for 24 h at RT. After removal of the solvent, the crude product was washed with freshly distilled pentane (2 x 40 mL). Precipitation from a CH_2Cl_2/pentane mixture afforded pure **3** as a light brown powder in 63 % yield (670 mg, 0.5 mmol). ^{31}P NMR (120 MHz, $CDCl_3$): δ 36.8 (s, PPh_2). ^{1}H NMR (300 MHz, $CDCl_3$): δ 7.35–7.11 (m, 41H), 5.65 (d, 1H, $^3J_{HH}$ = 3.7 Hz), 4.65 (s, 1H), 4.26 (m, 2H), 2.91 (m, 8H), 1.06 (m, 2H), 0.07 (s, 9H). ^{13}C NMR (100 MHz, CD_2Cl_2): δ 360.5, 198.2, 163.5, 161.5,

136.0, 134.6, 134.1, 133.8, 133.7, 133.1, 132.1, 131.9, 131.7, 131.6, 131.5, 131.2, 129.6, 129.4, 129.0, 128.8, 128.7, 126.8, 126.4, 125.5, 124.6, 124.0, 121.8, 119.7, 103.2, 63.3, 29.0, 17.3, -1.4. HR-MS FD+ (m/z): 1185.2146 ($[M]^+$, calcd. 1185.2092 for $[C_{64}H_{64}ClO_2SP_4RuSi]^+$). FT-IR (KBr): $\nu_{=C=C}$ = 1623 cm^{-1}.

Synthesis of 4—To a solution of **3** (335 mg, 0.25 mmol, 1 equiv.), $NaPF_6$ (84 mg, 0.5 mmol, 2 equiv.) and 1,1-diphenyl-2-propyn-1-ol (104 mg, 0.5 mmol, 2 equiv.) in dry CH_2Cl_2 (30 mL) under nitrogen atmosphere, was added Et_3N (140 µl, 1 mmol, 4 equiv.). The solution was stirred at RT for 48 h. The reaction mixture was washed with water and evaporated to dryness. The resulting solid was afterward washed with pentane and dried to afford **4** as a deep blue powder in 80 % yield (296 mg, 0.20 mmol). ^{31}P NMR (120 MHz, $CDCl_3$): δ 43.7 (s, PPh_2), -144.2 (sept, PF_6). ^1H NMR (300 MHz, $CDCl_3$): δ 7.66 (t, 2H, $^3J_{HH}$ = 7.4 Hz), 7.65 (d, 1H, $^3J_{HH}$ = 3.7 Hz), 7.24–7.16 (m, 18H), 7.04-6.78 (m, 30H), 6.37 (d, 1H, $^3J_{HH}$ = 6 Hz), 4.44 (m, 2H), 2.90 (m, 8H), 1.16 (m, 2H), 0.13 (s, 9H). ^{13}C NMR (100 MHz, CD_2Cl_2): δ 316.1, 210.2, 163.2, 162.1, 144.2, 135.1, 133.5, 133.3, 133.0, 132.9, 132.6, 131.7, 131.1, 130.9, 130.7, 130.5, 129.2, 128.6, 128.3, 127.7, 63.5, 29.2, 17.4, -1.4. HR-MS FD+ (m/z): 1339.3087 ($[M]^+$, calcd. 1339.3094 for $[C_{79}H_{73}O_2SP_4RuSi]^+$). FT-IR (KBr): $\nu_{C\equiv C}$ = 2062 cm^{-1}, $\nu_{=C=C=C}$ = 1925, $\nu_{C=O}$ = 1691 cm^{-1}, $\nu_{P\text{-}Ph}$ = 1088 cm^{-1}, $\nu_{P\text{-}F}$ = 839 cm^{-1}.

Synthesis of [Ru]1—To a solution of **4** (125 mg, 0.08 mmol, 1 equiv.) in dry THF (12 mL) under nitrogen atmosphere, was added tetrabutylammonium fluoride (163 µL, 1M in THF, 2 equiv.). The solution was stirred at RT for 20 h. After evaporation of the solvent, the resulting solid was dissolved in CH_2Cl_2 and the solution was washed with 10 % aqueous citric acid and water. The solvent was evaporated and the solid was recrystallized by slow diffusion from a CH_2Cl_2/pentane solvent mixture to afford **[Ru]1** as a deep blue powder in 72 % yield (83 mg, 0.06 mmol). ^{31}P NMR (120 MHz, $CDCl_3$): δ 43.5 (s, PPh_2), -144.4 (sept, PF_6). ^1H NMR (300 MHz, CDCl3): δ 7.66 (t, 2H, $^3J_{HH}$ = 7.4 Hz), 7.61 (d, 1H, $^3J_{HH}$ = 3.7 Hz), 7.33–6.79 (m, 48H), 6.42 (d, 1H, $^3J_{HH}$ = 3.7 Hz), 3.01 (m, 4H), 2.80 (m, 4H). ^{13}C NMR (100 MHz, CD_2Cl_2): δ 316.0, 213.2, 165.9, 161.9, 144.6, 139.6, 135.5, 135.0, 133.8, 133.7, 133.6, 133.1, 133.0, 132.4, 131.1, 130.8, 130.7, 129.3, 128.6, 128.4, 127.9, 127.5, 29.5. HR-MS FD+ (m/z): 1239.2368 ($[M]^+$, calcd. 1239.2386 for $[C_{74}H_{61}O_2SP_4RuSi]^+$). FT-IR (KBr): $\nu_{C\equiv C}$ = 2039 cm^{-1}, $\nu_{=C=C=C}$ = 1917, $\nu_{C=O}$ = 1688 cm^{-1}, $\nu_{P\text{-}Ph}$ = 1094 cm^{-1}, $\nu_{P\text{-}F}$ = 837 cm^{-1}.

Synthesis of 6—In a Schlenk tube under inert atmosphere, $[RuCl(dppe)_2][TfO]$ (**1**) (1.08 g, 1 mmol, 1 equiv.) and **5** (0.67 g, 1.2 mmol, 1.2 equiv.) were dissolved in dry CH_2Cl_2 (50 mL). The mixture was stirred for 24 h at RT. After removal of the solvent, the crude product was washed with freshly distilled pentane (2 x 40 mL). Precipitation from a CH_2Cl_2/pentane mixture afforded pure **6** as a light brown powder in 93% yield (1.52 g, 0.93 mmol). ^{31}P NMR (120 MHz, $CDCl_3$): δ 35.8 (s, PPh_2). ^1H NMR (300 MHz, $CDCl_3$): δ 7.87 (d, 4H, $^3J_{HH}$ = 8.7 Hz), 7.34–7.07 (m, 40H), 6.88 (d, 4H, $^3J_{HH}$ = 8.7 Hz), 6.24 (d, 2H, $^3J_{HH}$ = 8.1 Hz), 5.63 (d, 2H, $^3J_{HH}$ = 8.1 Hz), 4.93 (s, 1H), 4.40 (m, 4H), 2.92 (m, 8H), 1.12 (m, 4H), 0.08 (s, 18H). ^{13}C NMR (100 MHz, CD_2Cl_2): δ 360.5, 166.6, 151.1, 144.2, 134.7, 134.5, 133.9, 133.1, 132.1, 131.9, 131.7, 131.6, 131.5, 131.2, 129.6, 129.4, 129.0, 128.8, 128.7,

126.8, 126.4, 125.5, 124.6, 124.0, 123.2, 122.8, 109.7, 63.6, 29.4, 17.9, -1.1. HR-MS FD+ (m/z): 1490.3749 ($[M]^+$, calcd. 1490.3876 for $[C_{84}H_{87}ClNO_4P_4RuSi_2]^+$). FT-IR (KBr): $\nu_{=C=C}$ = 1630 cm^{-1}.

Synthesis of 7—To a solution of **6** (164 mg, 0.1 mmol, 1 equiv.), $NaPF_6$ (34 mg, 0.2 mmol, 2 equiv.) and 1,1-diphenyl-2-propyn-1-ol (42 mg, 0.2 mmol, 2 equiv.) in dry CH_2Cl_2 (10 mL) under nitrogen atmosphere, was added Et_3N (60 µl, 4 equiv.). The solution was stirred at RT for 48 h. The reaction mixture was diluted with CH_2Cl_2 up to 30 mL. The organics were washed with water and evaporated to dryness. The resulting solid was afterward washed with pentane and dried to afford **7** as a deep blue powder in 89 % yield (160 mg, 0.089 mmol). ^{31}P NMR (120 MHz, $CDCl_3$): δ 43.3 (s, PPh_2), -144.2 (sept., PF_6). ^1H NMR (300 MHz, $CDCl_3$): δ 7.98 (d, 4H, $^3J_{HH}$ = 8.8 Hz), δ 7.87 (t, 2H, $^3J_{HH}$ = 7.4 Hz), 7.30–6.77 (m, 56H), 4.43 (m, 4H), 2.88 (m, 8H), 1.14 (m, 4H), 0.1 (s, 18H). ^{13}C NMR (100 MHz, CD_2Cl_2): δ 316.3, 212.9, 166.4, 162.4, 151.2, 144.7, 144.0, 140.9, 134.0, 133.8, 133.7, 133.5, 132.4, 131.4, 131.2, 130.9, 130.6, 129.4, 128.7, 128.3, 126.1, 125.3, 120.9, 63.4, 29.5, 17.7, -1.3. HR-MS FD+ (m/z): 1644.5029 ($[M]^+$, calcd. 1644.4899 for $[C_{99}H_{96}NO_4P_4RuSi_2]^+$). FT-IR (KBr): $\nu_{C\equiv C}$ = 2064 cm^{-1}, $\nu_{=C=C=C}$ = 1919, $\nu_{C=O}$ = 1706 cm^{-1}, $\nu_{P\text{-}Ph}$ = 1098 cm^{-1}, $\nu_{P\text{-}F}$ = 839 cm^{-1}.

Synthesis of [Ru]2—To a solution of **7** (250 mg, 0.140 mmol, 1 equiv.) in dry THF (30 mL) under nitrogen atmosphere, was added tetrabutylammonium fluoride (307 µL, 1M in THF, 2.2 equiv.). The solution was stirred at RT for 24 h. After evaporation of the solvent, the resulting solid was dissolved in CH_2Cl_2 and the mixture was washed with 10 % aqueous citric acid, pure water and then dried to afford **[Ru]2** as a deep blue powder in 76 % yield (179 mg, 0.106 mmol). ^{31}P NMR (120 MHz, CD_2Cl_2): δ 43.2 (s, PPh_2), -142.6 (sept., PF_6). ^1H NMR (300 MHz, CD_2Cl_2): δ 7.94 (d, 4H, $^3J_{HH}$ = 8.7 Hz), δ 7.64 (t, 2H, $^3J_{HH}$ = 7.4 Hz), 7.28–6.77 (m, 56H), 2.99 (m, 4H), 2.81 (m, 4H). ^{13}C NMR (100 MHz, CD_2Cl_2): δ 317.6, 214.1, 166.9, 162.6, 151.6, 145.1, 144.6, 141.6, 135.9, 135.4, 134.9, 134.6, 133.9, 132.6, 131.8, 131.6, 131.2, 130.7, 129.7, 129.3, 129.0, 128.6, 126.0, 125.3, 123.3, 121.5, 29.6. HR-MS ESI+ (m/z): 1444.3406 ($[M]^+$, calcd. 1444.3449 for $[C_{89}H_{72}NO_4P_4Ru]^+$). FT-IR (KBr): $\nu_{C\equiv C}$ = 2063 cm^{-1}, $\nu_{=C=C=C}$ = 1917, $\nu_{C=O}$ = 1714-1681 cm^{-1}, $\nu_{P\text{-}Ph}$ = 1095 cm^{-1}, $\nu_{P\text{-}F}$ = 838 cm^{-1}.

Computational details

All the calculations have been performed with the Gaussian09 suite of programs for quantum chemistry.[37] We employed the PBE0 hybrid density functional[38] for ground state calculations, including the semi-empirical dispersion term proposed by Grimme (D3BJ).[39] The standard Pople's 6-31G(d,p) basis set,[40] for H, C, N, O, P, and S atoms, and the SDD effective core potential and basis set for Ru[41] provided the best compromise between accuracy and computational feasibility. The polarizable continuum model (PCM) of solvation[42] has been applied to model the dichloromethane solvent. The Ru-based dyes under investigation have been purposely designed to undergo electronic excitation with long-range intra-molecular charge-transfer from the ground to the excited states. This represents the worst-case scenario for state-of-the-art time-dependent DFT (TD-DFT) methods.[43] Thus we tested several density functional models for the TD-DFT calculations (see Table S1

Europe PMC Funders Author Manuscripts

in Supporting Information) and we chose the long-range corrected LC-ωPBE density functional.[44] Analysis of electron density rearrangement upon vertical excitation has been performed according to the charge-transfer indexes developed by Ciofini and coworkers.[32]

Electrode preparation method

NiO electrodes (thickness 1.5 μm) on TCO glass were purchased from Dyenamo AB, Stockholm, Sweden. UV-visible absorbance spectra of the sensitized films were recorded on an Agilent Cary 60 UV-Vis spectrometer equipped with a solid sample holder.

Film sensitization—NiO electrodes were soaked into a 0.5 mM solution of **[Ru]1** or **[Ru]2** in MeCN for 24h on an orbital stirring table. The electrodes were rinsed with MeCN and dried in air.

Photoelectrochemical measurements—Chrono-amperometric and linear sweep voltammograms were measured with a Bio-logic SP 300 potentiostat under nitrogen at room temperature using a previously described specific cell in three-electrode configuration.[15] The NiO electrode is clamped on the cell, serving both as working electrode and window. The surface of the working electrode in contact with the electrolyte is 0.42 cm^2. Ti wire and Ag/AgCl (KCl 3M) have been used as counter-electrode and reference electrode, respectively. We used potassium phosphate buffer (0.1M; pH = 7) as electrolyte and $[Co(NH_3)_5Cl]Cl_2$ (20 mM) as irreversible electron acceptor. The $[Fe(CN)_6]^{3-}/[Fe(CN)_6]^{4-}$ couple (E^0 = 0.244 V *vs.* Ag/AgCl, referred at 0.425 V *vs.* NHE in 0.1 M potassium phosphate buffer (0.1M; pH = 7) as electrolyte and $[Co(NH_3)_5Cl]Cl_2$ (20 mM) as irreversible electron acceptor. The $[Fe(CN)_6]^{3-}/[Fe(CN)_6]^{4-}$ couple (E^0 = 0.244 V vs. Ag/AgCl, referred at 0.425 V vs. NHE in 0.1 M potassium phosphate buffer at pH = 7; E^0 = 0.200 V *vs.* Ag/AgCl, referred at 0.412 V *vs.* NHE in 0.1 M sodium acetate buffer at pH = 4.5)[45] was then used for the standardization of the measurements in aqueous solution. Photoelectrodes were back-illuminated with a 300 W ozone-free xenon lamp (Newport) operated at 280 W, coupled to a water-filled Spectra-Physics 6123NS liquid filter for elimination of IR radiation (λ > 800 nm) and a Spectra-Physics 59472 UV cut-off filter (λ > 400 nm). Irradiance at the substrate surface was calibrated at 100 mW cm^{-2} using the Newport PM1918-R power-meter.

Supplementary Material

Refer to Web version on PubMed Central for supplementary material.

Acknowledgements

This work was supported by the French National Research Agency (Labex program, ARCANE, ANR-11-LABX-0003-01 and ANR-14-CE05-0013 (CORuS project)) and the European Research Council under the European Union's Seventh Framework Program (FP/2007-2013)/ERC Grant Agreement n.306398. The authors thank Drs. Nathan McClenaghan and Serguey Denisov for help with spectroscopy measurements.

Notes and references

1. Faunce TA, Lubitz W, Rutherford AW, MacFarlane D, Moore GF, Yang P, Nocera DG, Moore TA, Gregory DH, Fukuzumi S, Yoon KB, et al. Energy Environ Sci. 2013; 6:695–698.

2. Faunce T, Styring S, Wasielewski MR, Brudvig GW, Rutherford AW, Messinger J, Lee AF, Hill CL, deGroot H, Fontecave M, MacFarlane DR, et al. Energy Environ Sci. 2013; 6:1074–1076.
3. Thapper A, Styring S, Saracco G, Rutherford AW, Robert B, Magnuson A, Lubitz W, Llobet A, Kurz P, Holzwarth A, Fiechter S, et al. Green. 2013; 3:43–57.
4. Walter MG, Warren EL, McKone JR, Boettcher SW, Mi Q, Santori EA, Lewis NS. Chem Rev. 2010; 110:6446–6473. [PubMed: 21062097]
5. McKone JR, Lewis NS, Gray HB. Chem Mater. 2014; 26:407–414.
6. Queyriaux N, Kaeffer N, Morozan A, Chavarot-Kerlidou M, Artero V. J Photochem Photobiol C: Photochemistry Reviews. 2015; 25:90–105.
7. Yu Z, Sun L. Energy Environ Sci. 2015; 8:760–775.
8. Odobel F, Le Pleux L, Pellegrin Y, Blart E. Acc Chem Res. 2010; 43:1063–1071. [PubMed: 20455541]
9. Odobel F, Pellegrin Y. J Phys Chem Lett. 2013; 4:2551–2564.
10. Li L, Duan L, Wen F, Li C, Wang M, Hagfeldt A, Sun L. Chem Commun. 2012; 48:988–990.
11. Tong L, Iwase A, Nattestad A, Bach U, Weidelener M, Götz G, Mishra A, Bäuerle P, Amal R, Wallace GG, Mozer AJ. Energy Environ Sci. 2012; 5:9472–9475.
12. Ji Z, He M, Huang Z, Ozkan U, Wu Y. J Am Chem Soc. 2013; 135:11696–11699. [PubMed: 23895560]
13. Fan K, Li F, Wang L, Daniel Q, Gabrielsson E, Sun L. PhysChemChemPhys. 2014; 16:25234–25240.
14. Li F, Fan K, Xu B, Gabrielsson E, Daniel Q, Li L, Sun L. J Am Chem Soc. 2015; 137:9153–9159. [PubMed: 26132113]
15. Massin J, Bräutigam M, Kaeffer N, Queyriaux N, Field MJ, Popp J, Chavarot-Kerlidou M, Dietzek B, Artero V. Interface Focus. 2015; 5:20140083. [PubMed: 26052420]
16. Wood CJ, Summers GH, Clark CA, Kaeffer N, Braeutigam M, Carbone LR, D'Amario L, Fan K, Farré Y, Narbey S, Oswald F, et al. Phys Chem Chem Phys. 2016; 18:10727–10738. [PubMed: 26734947]
17. De Sousa S, Ducasse L, Kauffmann B, Toupance T, Olivier C. Chem Eur J. 2014; 20:7017–7024. [PubMed: 24753075]
18. De Sousa S, Lyu S, Ducasse L, Toupance T, Olivier C. J Mater Chem A. 2015; 3:18256–18264.
19. Lyu S, Farré Y, Ducasse L, Pellegrin Y, Toupance T, Olivier C, Odobel F. RSC Adv. 2016; 6:19928–19936.
20. Touchard D, Haquette P, Daridor A, Romero A, Dixneuf PH. Organometallics. 1998; 17:3844–3852.
21. Olivier C, Kim BS, Touchard D, Rigaut S. Organometallics. 2008; 27:509–518.
22. Winter RF, Klinkhammer KW, Zalis S. Organometallics. 2001; 20:1317–1333.
23. Pélerin O, Olivier C, Roisnel T, Touchard D, Rigaut S. J Organomet Chem. 2008; 693:2153–2158.
24. Inzelt, G.Lewenstam, A., Scholz, F., editors. Handbook of reference electrodes. Table 6.2. Springer-Verlag; Berlin Heidelberg: 2013. p. 158
25. Huan TN, Andreiadis ES, Heidkamp J, Simon P, Derat E, Cobo S, Royal G, Bergmann A, Strasser P, Dau H, Artero V, et al. J Mater Chem A. 2015; 3:3901–3907.
26. Weidelener M, Powar S, Kast H, Yu Z, Boix PP, Li C, Müllen K, Geiger T, Kuster S, Nüesch F, Bach U, et al. Chem Asian J. 2014; 9:3251–3263. [PubMed: 25234556]
27. Boschloo G, Hagfeldt A. J Phys Chem B. 2001; 105:3039–3044.
28. Weidelener M, Mishra A, Nattestad A, Powar S, Mozer AJ, Mena-Osteritz E, Cheng Y-B, Bach U, Bäuerle P. J Mater Chem. 2012; 22:7366–7379.
29. Gross MA, Creissen CE, Orchard KL, Reisner E. Chem Sci. 2016; doi: 10.1039/c6sc00715e
30. Chen W, Rein FN, Rocha RC. Angew Chem Int Ed. 2009; 48:9672–9675.
31. Pellegrin Y, Le Pleux L, Blart E, Renaud A, Chavillon B, Szuwarski N, Boujtita M, Cario L, Jobic S, Jacquemin D, Odobel F. J Photochem Photobiol A. 2011; 219:235–242.
32. Le Bahers T, Adamo C, Ciofini I. J Chem Theory Comput. 2011; 7:2498–2506. [PubMed: 26606624]

33. Munoz-Garcia AB, Pavone M. Phys Chem Chem Phys. 2015; 17:12238–12246. [PubMed: 25892559]
34. Hamd W, Chavarot-Kerlidou M, Fize J, Muller G, Leyris A, Matheron M, Courtin E, Fontecave M, Sanchez C, Artero V, Laberty-Robert C. J Mater Chem A. 2013; 1:8217–8225.
35. We note that such values are much lower to those typically measured in non-aqueous electrolytes as previously reported: Bella F, Gerbaldi C, Barolo C, Grätzel M. Chem Soc Rev. 2015; 44:3431–3473. [PubMed: 25864577]
36. Fox MA, Harris JE, Heider S, Pérez-Gregorio V, Zakrzewska ME, Farmer JD, Yufit DS, Howard JAK, Low P. J Organomet Chem. 2009; 694:2350–2358.
37. Frisch, MJ., Trucks, GW., Schlegel, HB., Scuseria, GE., Robb, MA., Cheeseman, JR., Scalmani, G., Barone, V., Mennucci, B., Petersson, GA., Nakatsuji, H., et al. Gaussian 09, Revision D.01. Gaussian, Inc.; Wallingford CT: 2009.
38. Adamo C, Barone V. J Chem Phys. 1999; 110:6158–6169.
39. Grimme S, Ehrlich S, Goerigk L. J Comp Chem. 2011; 32:1456–1465. [PubMed: 21370243]
40. Rassolov VA, Ratner MA, Pople JA, Redfern PC, Curtiss LA. J Comp Chem. 2001; 22:976–984.
41. Andrae D, Haeussermann U, Dolg M, Stoll H, Preuss H. Theor Chem Acc. 1990; 77:123–141.
42. Scalmani G, Frisch MJ. J Chem Phys. 2010; 132:114110. [PubMed: 20331284]
43. Dreuw A, Head-Gordon M. J Am Chem Soc. 2004; 126:4007–4016. [PubMed: 15038755]
44. Vydrov OA, Scuseria GE. J Chem Phys. 2006; 125:234109. [PubMed: 17190549]
45. O'Reilly JE. Biochim Biophys Acta. 1973; 292:509–515. [PubMed: 4705442]

Europe PMC Funders Author Manuscripts

Europe PMC Funders Author Manuscripts

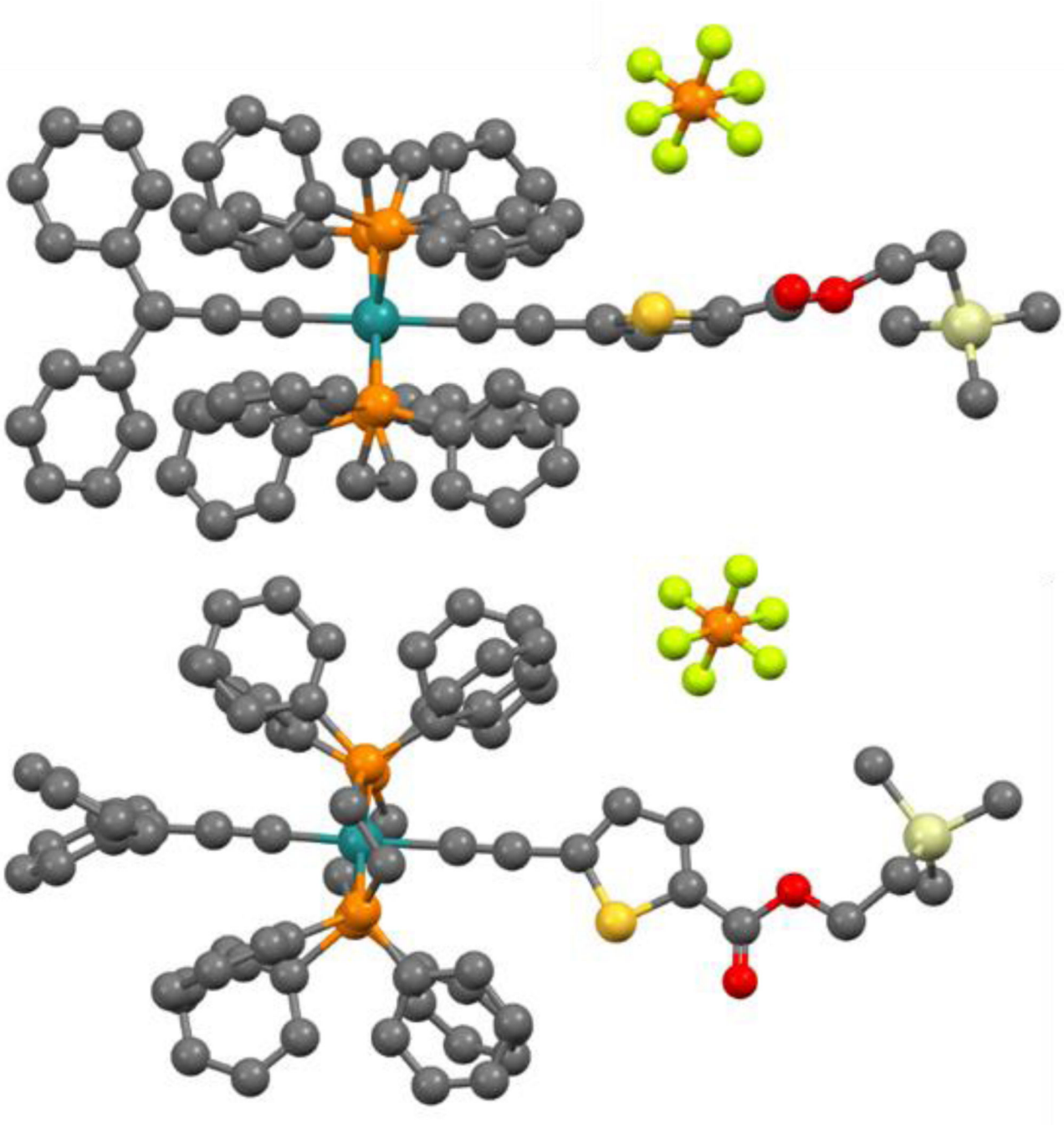

Fig. 1.
Crystal structure of **4** (top and side views). Proton and solvent molecules were removed for clarity.

Europe PMC Funders Author Manuscripts

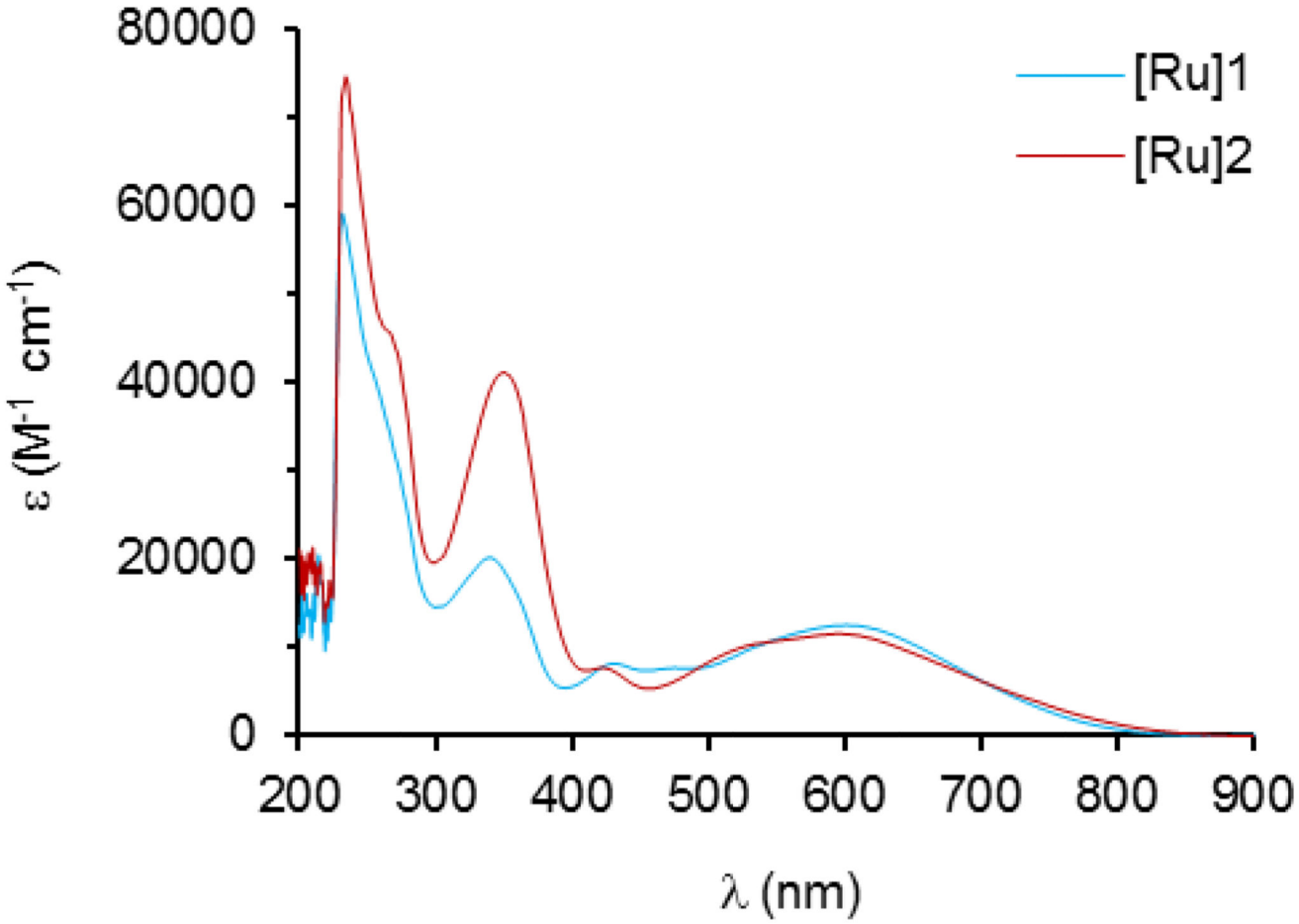

Fig. 2.

Absorption spectra of **[Ru]1** (blue line) and **[Ru]2** (red line) in CH_2Cl_2 (C ˜ 3.10^{-5} M ; optical pathway 1 cm).

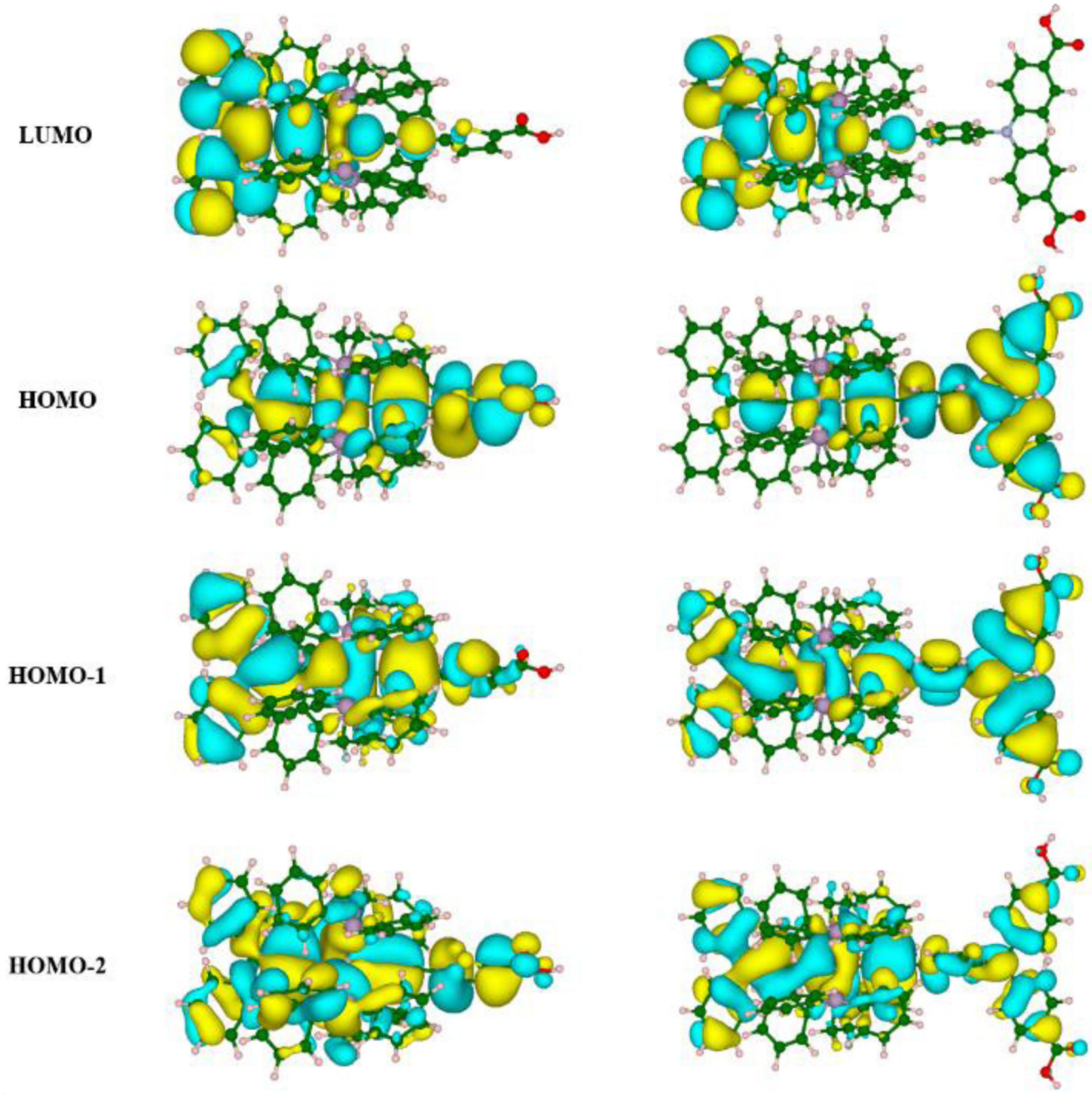

Fig. 3.
Electron-density distribution of the transition-involved frontier molecular orbitals of **[Ru]1** (left) and **[Ru]2** (right).

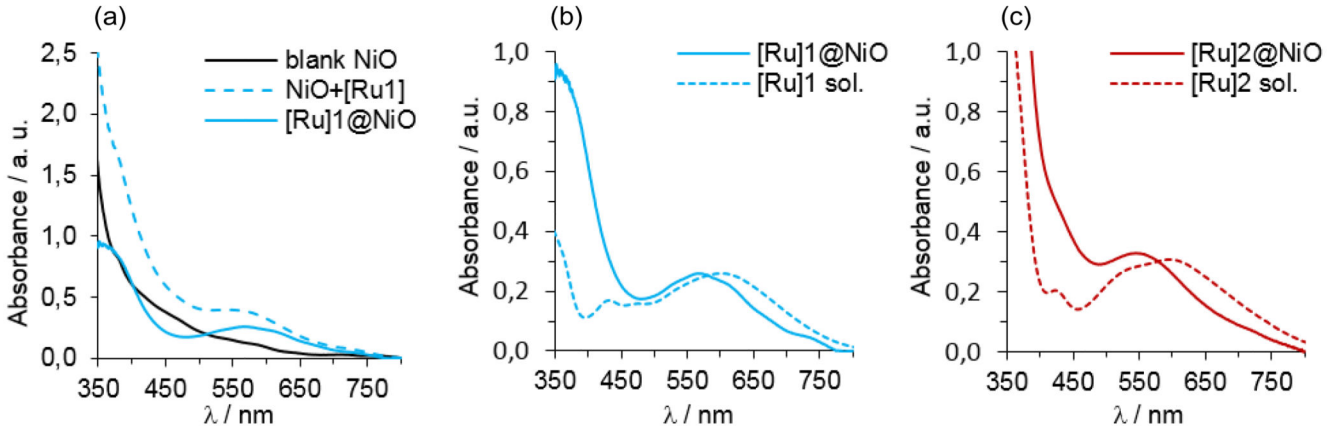

Fig. 4.

(a) Absorbance spectra of a blank NiO electrode (black line) and of the same electrode after sensitization with **[Ru]1** (dashed blue line). The difference between these two spectra is shown as a plain blue line. (b) Comparison of corrected spectra recorded on NiO film (plain blue line) and CH_2Cl_2 (C ˜ 3.10^{-5} M; optical pathway 1 cm) solution spectra of **[Ru]1** (dashed blue line). (c) Comparison of corrected spectra recorded on NiO film (plain red line) and CH_2Cl_2 (C ˜ 3.10^{-5} M; optical pathway 1 cm) solution spectra of **[Ru]2** (dashed red line).

Europe PMC Funders Author Manuscripts

Europe PMC Funders Author Manuscripts

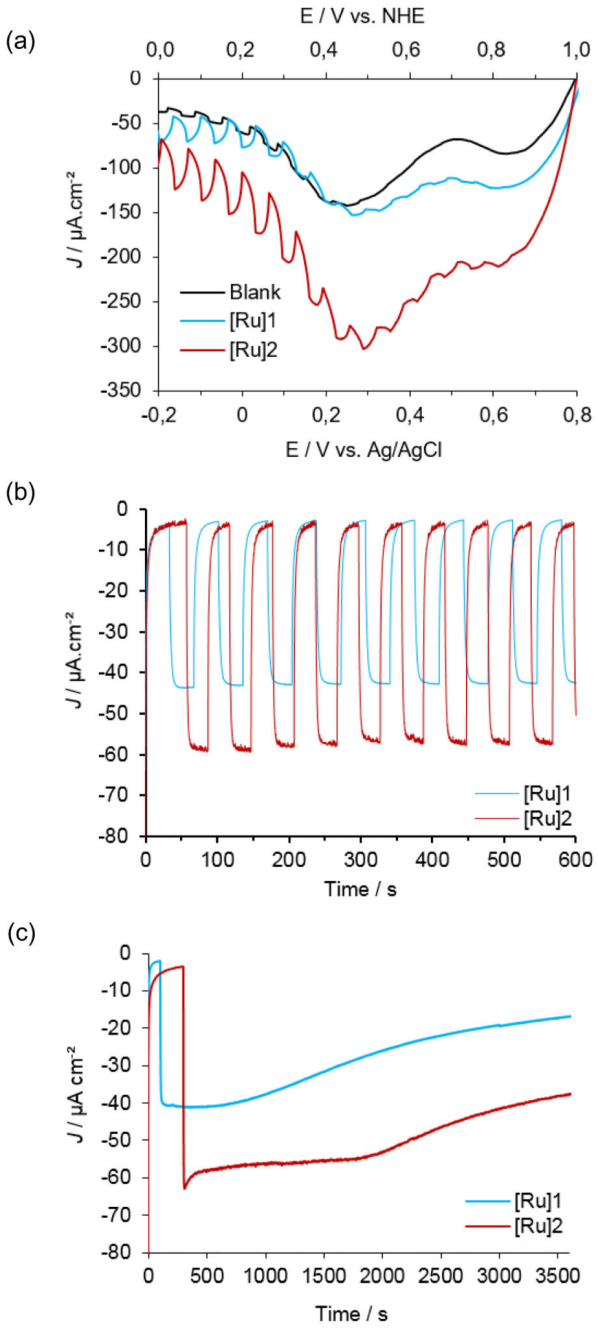

Fig. 5.

(a) Linear sweep voltammograms (10 mV s^{-1}) recorded under chopped-light on a non-sensitized NiO electrodes (black line) or NiO electrodes sensitized with **[Ru]1** (blue line) or **[Ru]2** (red line) in the presence of $[Co(NH_3)_5Cl]Cl_2$ (20 mM). (b) Cathodic photocurrent measurements recorded for 10 minutes under chopped-light NiO electrodes sensitized with **[Ru]1** (blue line) or **[Ru]2** (red line) in the presence of $[Co(NH_3)_5Cl]Cl_2$ (20 mM) in phosphate buffer (0.1 M ; pH 7) at + 0.2 V vs. NHE. (c) Cathodic photocurrent measurement recorded for 1 hour on NiO electrodes sensitized with **[Ru]1** (blue line) or **[Ru]2** (red line)

in the presence of $[Co(NH_3]_5Cl]Cl_2$ (20 mM) at + 0.2 V vs. NHE in phosphate buffer (0.1 M ; pH 7).

Europe PMC Funders Author Manuscripts

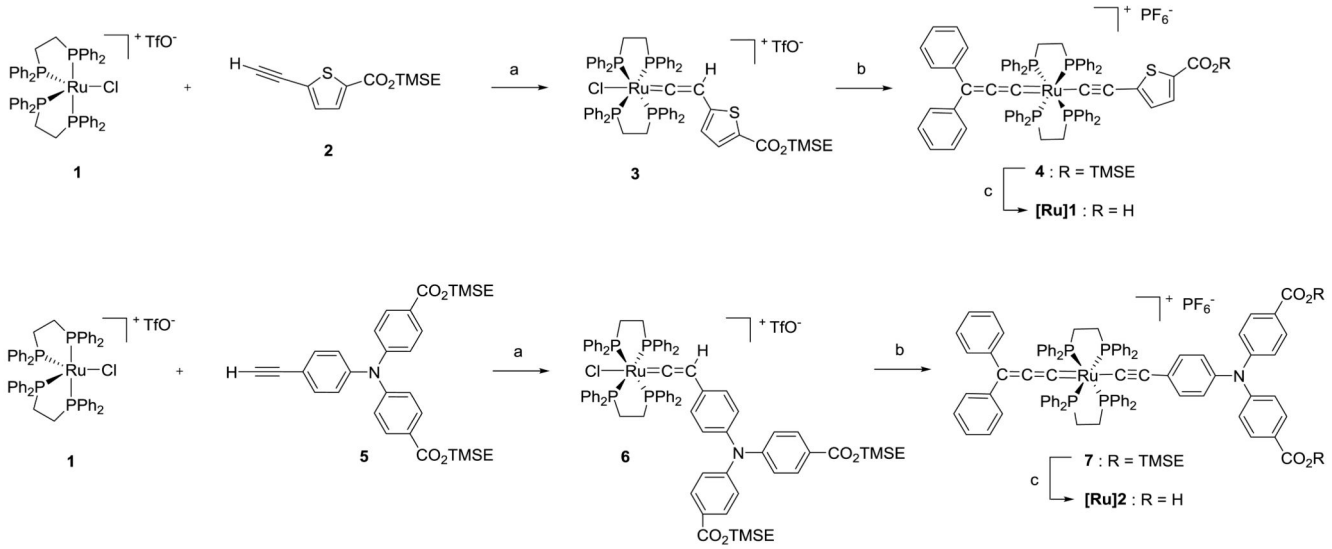

Scheme 1.

Synthetic routes to **[Ru]1** and **[Ru]2**. Conditions: (a) CH_2Cl_2; (b) Diphenyl-2-propyn-1-ol, $NaPF_6$, Et_3N, CH_2Cl_2; (c) Tetrabutylammonium fluoride, THF.

Europe PMC Funders Author Manuscripts

Europe PMC Funders Author Manuscripts

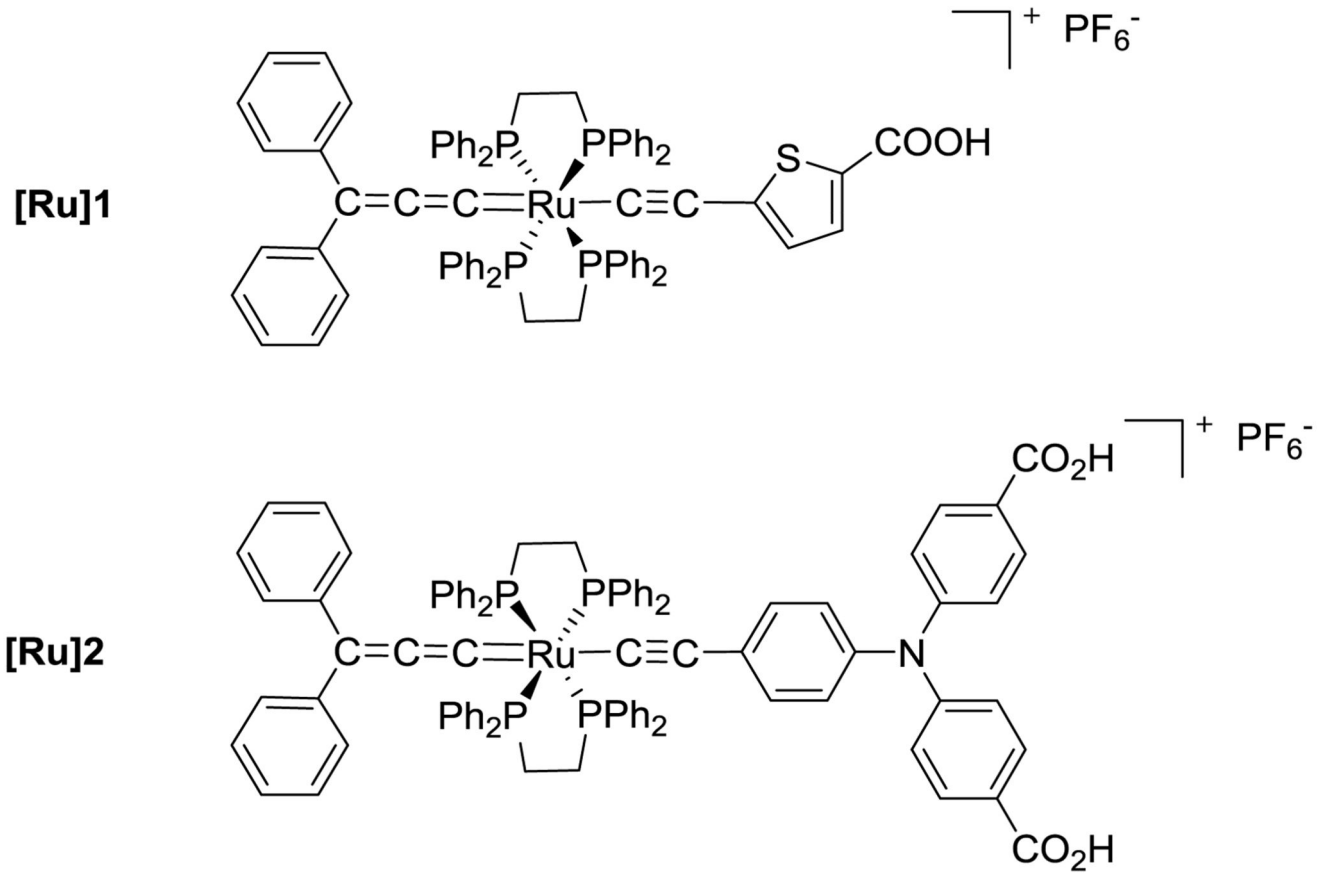

Chart 1.
Molecular structure of the dyes **[Ru]1** and **[Ru]2**.

Europe PMC Funders Author Manuscripts

Table 1

Optical and electrochemical properties.

Dye	λ_{max}/nm	ε/M^{-1} cm^{-1}	$E_{0\text{-}0}$/eV[a]	E_{Red}/V[b]	E_{LUMO}/V *vs.* NHE[c]	E_{LUMO}/eV[d]	E_{HOMO}/V *vs.* NHE[e]	E_{HOMO}/eV[f]
[Ru]1	602	12 500	1.58	– 0.99	– 0.46	– 4.11	+ 1.12	– 5.69
	340	20 100						
[Ru]2	598	11 500	1.53	– 0.89	– 0.36	– 4.21	+ 1.17	– 5.74
	350	41 000						

Absorption spectra and cyclic voltammograms recorded in CH_2Cl_2.

[a] 0-0 transition energy estimated from the onset of the absorption spectra.

[b] Reduction potential in V *vs.* Fc^+/Fc.

[c] Estimated LUMO level in V *vs.* NHE, obtained from the reduction potential considering E^0(Fc+/Fc) = + 0.53 *vs.* NHE.[15,25]

[d] Estimated LUMO energy in eV, considering $E^0_{(Fc+/Fc)}$ = – 5.1 eV.[26]

[e] Estimated HOMO level in V *vs.* NHE, obtained from $E_{LUMO}+E_{0\text{-}0}$.

[f] Estimated HOMO energy in eV, obtained from $E_{LUMO}-E_{0\text{-}0}$.

Europe PMC Funders Author Manuscripts

Table 2

DFT and TD-DFT calculated electronic properties in CH_2Cl_2.

Dye	ΔE_{calc}/eV[a]	λ_{calc}/nm[b]	f[c]	Transition assignment[d]	q_{CT}/e	D_{CT}/Å	$E_{HOMO\ calc.}$/eV[e]
[Ru]1	1.83	676	0.005	HOMO → LUMO ; HOMO-2 → LUMO	0.961	1.98	– 5.66
	2.93	423	0.841	HOMO-1 → LUMO			
[Ru]2	1.80	687	0.005	HOMO → LUMO	0.965	2.06	– 5.39
	2.93	423	0.856	HOMO-1 → LUMO ; HOMO-2 → LUMO			

[a] ΔE_{calc} = main transition energy.

[b] λ_{calc} = calculated λ_{max}.

[c] f = oscillator strength.

[d] Only the transitions with coefficients higher than 0.15 are given.

[e] $E_{HOMO\ calc.}$ = calculated energy of the HOMO.